2014 IEEE International Conference on Robotics & Automation (ICRA)
Hong Kong Convention and Exhibition Center
May 31 - June 7, 2014. Hong Kong, China

Development of a Large Area Scanner for Intraoperative Breast Endomicroscopy

Siyang Zuo, Michael Hughes, Petros Giataganas, Carlo Seneci, Tou Pin Chang, and Guang-Zhong Yang, *Fellow, IEEE*

***Abstract*— Recent work on probe-based confocal endomicroscopy has demonstrated its potential role for real-time assessment of tumour margins during breast conserving surgery. However, endomicroscope probes tend to have a very small field-of-view, making surveillance of large areas of tissue difficult, and limiting practical clinical deployment. In this paper, a new robotic device for controlled, large area scanning based on a fibre bundle endomicroscope probe is proposed. The prototype uses a 2-DOF mechanism (-90 to +90 degrees bending on one axis, 360 degrees of rotation on a second axis) as well as a passive linear structure to conform to undulating surfaces. Both axes are driven by brushless DC servo motors with computer control, thus facilitating large field-of-view mosaicing. Experimental results have shown good repeatability and low hysteresis of the device, which is able to scan different surface trajectories (e.g. a spiral pattern over a hemi-spherical surface) with consistent tissue contact. *Ex vivo* human breast tissue results are demonstrated, illustrating a viable scanning approach for breast endomicroscopy.**

I. Introduction

Breast cancer is currently the second leading cause of death of women in Europe [1]. Smaller cancers are often treated by breast conserving surgery (wide local excision), a procedure to remove the tumour and a surrounding cuff of normal tissue while leaving the remainder of the breast intact [2]. Currently, definitive assessment of whether the tumour has been completely excised can only be made post-operatively through histology. If the margins of the excised tissue are found to contain cancer cells (known as 'positive' margins), then this implies that the tumour has not been entirely removed, and that there is a high risk of cancer recurrence [3]. The patient will often be required to return to theatre for a second operation. This carries a further risk of postoperative infections, has a negative impact on cosmesis, and increases costs due to longer stays in hospital [4].

In the UK, the proportion of patients with positive surgical margins ranges from 20% to 40% [3, 5] and the national reoperation rates are 30% for non-invasive and 18% for invasive breast cancer [6]. These high reoperation rates suggest that a real-time, intraoperative technique for confirming complete removal of the cancer during surgery itself could have a significant impact on patient outcomes. Unfortunately, existing techniques such as gross examination by palpation [7] and intraoperative radiography on specimens [8] are not reliable. Frozen sections (a faster alternative to histology) can be used for intraoperative evaluation while the patient remains anaesthetized, but are rarely performed as they are costly, prolong the surgery [9], and are less reliable for the evaluation of non-invasive or small cancers [10].

Fluorescence confocal endomicroscopy [11], a cellular scale endoscopic imaging technique, is a candidate technology for real-time assessment of breast tumour margins. Confocal microscopy is distinguished from conventional microscopy by its ability to reject out-of-focus background light. This makes it suitable for use *in vivo*, where thick tissue must necessarily be imaged. Several groups have already considered bench-top confocal microscopy for analysis of breast tissues (for example [12]), and confocal endomicroscopy has also recently been suggested [13]. These results have indicated that it is possible to visualize key morphological structures of normal and cancerous breast tissue. Unlike bench-top microscopy, endomicroscopy could potentially be used directly on the internal surface of the breast cavity created during surgery rather than on *ex vivo* tissue samples.

In fluorescence confocal endomicroscopy, tissue is first stained using either topical or intravenous fluorescent contrast agents such as acriflavine hydrochloride and sodium fluorescein respectively. An image is then assembled in a point-by-point fashion by scanning a laser beam over the tissue surface. This scanning, which is a necessary feature of confocal microscopy, must be performed at high speed in order to achieve useful frame rates. The difficulties associated with miniaturizing high-speed scanners [11] have led to the development of fibre-bundle based endomicroscopes. Cellvizio by Mauna Kea Technologies, for example, can be used to identify characteristic morphological features of neoplastic and non-neoplastic changes of the gastrointestinal tract [14], biliary strictures [14] and lung [15]. A range of other applications have also been considered, and recently the potential for confocal endomicroscopy to image benign and malignant morphological features of breast tissues, and so to be used as a form of intraoperative surgical guidance, has been suggested [13].

One limitation arising from the use of fibre bundles is a trade-off between lateral resolution and field-of-view. Fibre bundles contain a finite number of cores (typically 30,000), which essentially act as pixels in the image. Whilst high-resolution endomicroscopy is possible through the use of non-unity magnification optics at the distal tip of the fibre bundle, the result is always a proportional reduction in the field-of-view. High-resolution fibre bundle endomicroscopes (e.g. Cellvizio UHD probes) are limited in field-of-view to the order of 240 μm, making surveillance of large areas of tissue difficult.

Siyang Zuo, Michael Hughes, Petros Giataganas, Carlo Seneci, Tou Pin Chang, and Guang-Zhong Yang are with the Hamlyn Centre for Robotic Surgery, Imperial College London, SW7 2AZ, London, UK (email: s.zuo@imperial.ac.uk).

The effective field-of-view can be increased by mosaicing: stitching together of adjacent image frames as the probe is moved across the tissue [16-19]. This tends to be rather difficult to perform, requiring careful control of the probe over small scales. In practice, manual handling of large area coverage can be difficult and time consuming, thus motivating the development of mechanical scanning devices which could translate the endomicroscope probe smoothly over a 2D area.

Our early work was focused on the development of an articulated robot for the general manipulation of biophotonics probes for minimally invasive surgery [20]. Recent developments in this research area include a scanning device by Rosa et al., which employs hydraulic micro-balloons [21], and one by Erden et al., using a conic structure [22]. A force-adaptive motion control approach has been proposed by Newton et al., which uses an articulated robotic endoscope [23], a handheld device by Latt et al. [24], or a cooperative robotic arm [25] to generate a 3D map of the tissue. Attention has also been paid to solving the difficulties associated with scanning over large areas of deformable tissue and reliably assembling mosaics [26-28].

The solutions described in [21] and [22] were targeted at applications for which the scanning device must firstly remain very compact, and secondly must be flexible. As a result, only relatively small areas of tissue could be mosaiced. The requirements for a scanner for imaging the breast cavity are somewhat different, with ergonomic constraints relaxed, but with a need to scan over a large, 3D curved surface [25]. Studies so far which have shown large area mosaics using mechanized scanning of endomicroscope probes [25, 28] involved complex robotic systems that could not easily be adapted to *in vivo* clinical use. This application therefore requires a new device which is capable of scanning over a much larger area of tissue, in a more reliable and repeatable manner, but with simpler mechatronics.

To this end, we have developed a prototype device which would allow scanning over the internal surface of the breast cavity. The scanner is designed to be inserted through the incision created during breast conserving surgery. When the scanner approaches the target imaging area, the tissue surface is shaped to a smooth surface by a thin transparent plastic membrane attached to the scanner. The device then smoothly scans the endomicroscope probe over a large, 2D area of tissue, allowing a mosaic to be assembled.

In this paper, a prototype of the scanner with 2 degrees of freedom (DOF) scanning mechanism and a 1-DOF passive linear structure is described. In the following sections, we include: 1) a description of the novel mechanical design, 2) integration with the endomicroscope and mosaicing software, 3) mechanical performance analysis, 4) mosaicing experiments and 5) results of *ex vivo* human breast tissue experiments to evaluate the potential of this device for breast endomicroscopy.

II. Design Concept

A. 2-DOF scanning mechanism

The device is able to scan over a 2D curved surface by bending and rotation of the distal tip. The distal structure consists of two cylindrical tube frames (tip and base), one pin joint, one spur gear link, and one rotation gear shaft (Fig. 1). The base and tip frames are linked via the pin joint, while the spur gear is fixed to the tip frame. The bending motion is driven by the rotation gear shaft which sits inside the base frame and engages with the spur gear. When the rotation gear shaft rotates by angle α, it provides the tip frame with a moment around the pin joint, thus achieving a bending angle of angle θ. The relation between α and θ is:

$$\theta = \frac{R}{r}\alpha$$

The rotational motion is achieved by rotating the base frame and the rotation gear tube at the same speed and in the same direction. Together with the bending motion, this provides the hemi-spherical workspace shown in Fig. 2. For example, a spiral trajectory can be achieved by rotating the base frame and rotation gear tube simultaneously at varying rotational speeds. The radial position h is related to the angles of rotation by:

$$h = Hsin(\frac{R}{r}(\beta - \alpha))$$

The angular position around the spiral is given by the rotational angle of the base frame (β).

B. Passive linear structure

The passive linear structure is shown in Fig. 3. It consists of the contact head, two freely rotating balls, a spring and the tip frame. The balls, which are embedded in the contact head, rotate during scanning, acting as wheels, while the spring ensures constant contact between the head and the tissue. This structure is designed to allow effective scanning over undulating surfaces.

A membrane is fixed to the support attachment. In breast endomicroscopy, this can be inserted into the breast cavity to reshape the uneven surface of the tissue. By ensuring consistent tissue contact, it creates a smooth surface for scanning. Provided the membrane is sufficiently thin, the finite working distance of endomicroscopy probes (which can easily be arranged to be of the order of several tens of microns) allows tissue to be imaged.

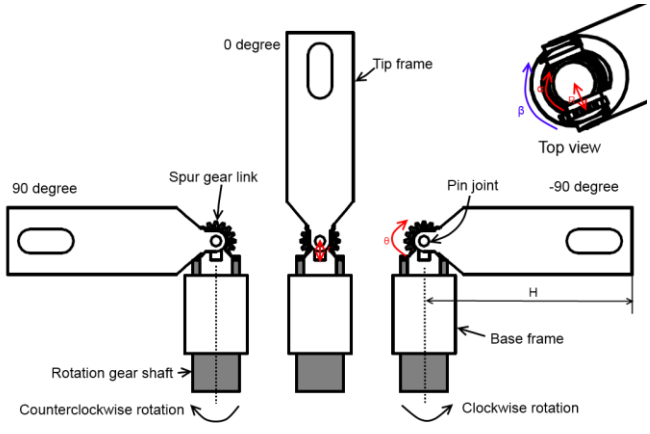

Figure 1. Bending mechanism, transforming rotational motion of the gear shaft to a rotation of the frame, enablinga ± 90 degrees bending motion.

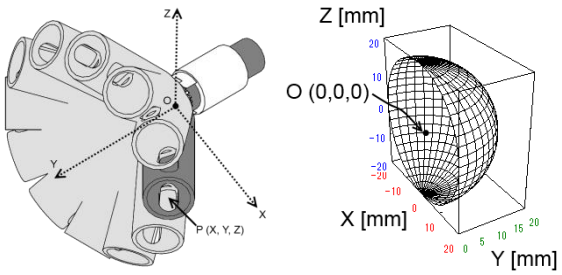

(a) (b)

Figure 2. Rotating mechanism, (a) Rotating model of bending distal end, (b) workspace of bending distal end.

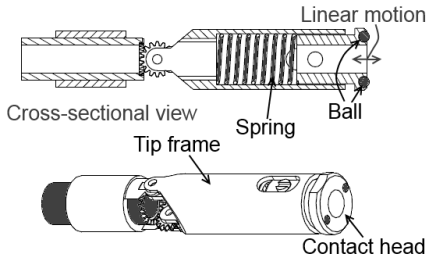

Figure 3. Passive linear structure.

III. System Architecture

The proposed hardware consists of the multi-DOF distal end, the driver unit, a computer-based control unit and a fibre bundle endomicroscope as shown in Fig. 4.

A. Multi-DOF distal end

The distal end has a 1-DOF bending and a 1-DOF rotating mechanism. The prototype has an outer diameter of 6 mm, and a length of 83 mm, while the bending tip has a length of 23 mm (Fig. 5). The prototype is equipped with one 3 mm diameter central channel, through which the endomicroscope probe can be passed. The distal end (except the contact tip) was fabricated from stainless steel, while the contact tip was rapid prototyped (VeroBlackPlus, Objet Geometries Ltd., Israel). The endomicroscope probe is passed through the 3 mm working channel of the scanner and fixed in place by a screw on the distal tip.

B. Driver unit

The rotation gear shaft and base frame, which are placed concentrically, bend and rotate the distal end using two brushless DC-servomotors (1226 E 012 B K1855, Fauhaber SA, Germany) with rotation gears (Fig. 5). A spring structure is located posterior to the rotation gear for minimizing the backlash between the rotation gear shaft and spur gear link. Hall effect sensors are used to detect the rotation angle of the shaft for the purposes of feedback control. The motion controllers have been integrated into the driver unit. The distal end is specifically separated from the driver unit, allowing it to be cleaned and sterilized.

C. User interface

A custom designed user interface has been developed to control the prototype from a standard PC. Once the scan parameters are entered, the device can scan the target surface automatically. These parameters include the linear velocity of the probe, the required number of turns in the spiral and the radial spacing between turns. For experimental purposes, the actual signal output of the motor, including rotation speed, and rotation angle, as well as the effective scan speed and scan area, are displayed and recorded. In future we intend to use this information to assist with the assembling of mosaics.

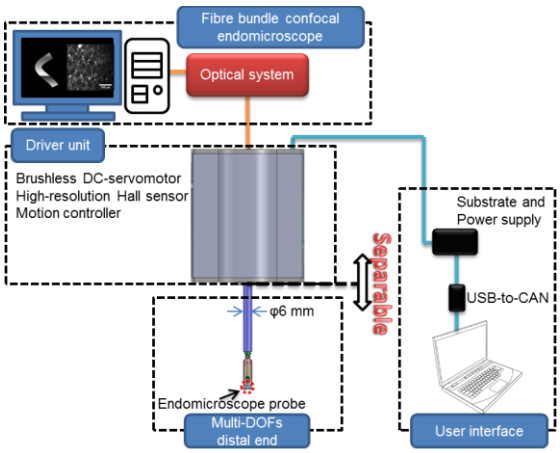

Figure 4. System configuration of scanner. The multi-DOFs distal end is sterilizable and separable from the driver unit

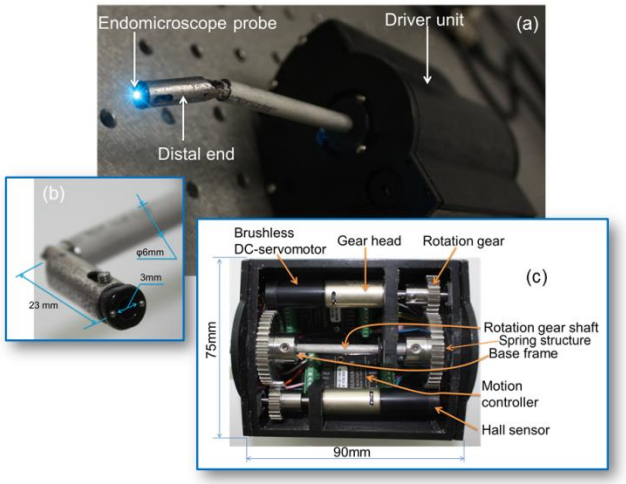

Figure 5. Prototype of the scanner. (a) The scanner with the endomicroscope probe inserted; (b) distal end showing dimensions; (c) details of the driver unit with rotation gear, brushless DC-servomotors, gear head and Hall sensor.

D. Fibre bundle confocal endomicroscope

The fibre-bundle and micro-lens assembly (the 'probe') used for this study are from a commercial endomicroscopy system (Cellvizio Gastroflex UHD, Mauna Kea Technologies), and were used with in-house laser scanning and image acquisition systems. This custom acquisition system allows a combination of imaging, mosaicing and scanner control for real-time use. The laser scanning system, which is similar to several others systems reported in the literature [11, 29, 30], uses a galvanometer mirror, a resonant scanning mirror and relay optics to scan a 488 nm laser beam over the proximal end of the fibre bundle. This scanning pattern is transferred to the tissue by the bundle and the distal optics, giving a usable circular field-of-view with a diameter of approximately 240 µm. Returning fluorescent emission is de-scanned by the same scanning system, diverted by a

dichroic mirror, and focused through a pinhole onto an avalanche photodiode (APD). The signal from the APD is digitized by a high-speed digitizer (National Instruments), and image frames are assembled using software developed in Labview (National Instruments). The honeycomb-like image structure arising from the fibre bundle is removed using a Gaussian spatial filter. Images are displayed live to the user at 10 frames per second, and also streamed to an uncompressed AVI.

E. Mosaicing software

For testing purposes, we implemented a simple, offline mosaicing algorithm in Matlab. Since the 2D motion of the scanner is partly achieved through rotation of the distal tip, we expect rotation between successive image frames in addition to a lateral translation. This rotation can be corrected for prior to mosaicing as follows. For initial experiments, we set the software to rotate each image frame by a number of trial angles (between 0 and 8 degrees in steps of 0.5 degrees) and computed the normalized 2D cross-correlation between each rotated image and the previous frame. The most likely rotation angle and lateral shift could then be calculated by searching for the cross correlation peak across the three dimensions. If the cross-correlation peak fell below a threshold (empirically set at 0.92 in this study), the shift and rotation was instead assumed to be the same as for the previous pair of frames. We did not use a blending algorithm - the new frame is simply copied to the mosaic in the estimated position, over-writing any existing pixels. The algorithm is therefore a simplified version of those previously reported for mosaicking of confocal and widefield endomicroscopy videos [16-19, 31]. The algorithm could be improved by attempting to correct for the raster scan formation of the images, and inevitable tissue deformation [27].

F. Trajectory Selection

The time taken to complete a scan would be an important consideration when translating this technology to the clinic. Given the fairly low (10 Hz) frame rate of the endomicroscopy system, it is important to cover the required scanning area as efficiently as possible. This is complicated by the need to ensure sufficient overlap between image frames for robust mosaicing. We found experimentally that a shift of 40 µm between images (i.e. an overlap of 200 µm) was necessary to ensure consistent results, implying a maximum acceptable linear velocity of 0.4 mm/s.

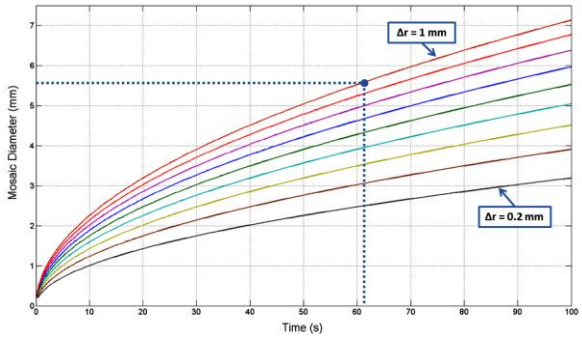

Figure 6. The diameter of the circular area that the device can scan over in a given time for values of the loop spacing Δr between 0.2 and 1 mm (in 0.1 mm steps). Note that a value below 0.24 mm would be required for a spiral without gaps.

While a large number of trajectories are possible, we selected a spiral path as an effective way of covering a circular scan area. (Selection of the optimum trajectory for different scan areas is a topic of further investigation). If the spacing between spiral loops is set at 0.24 mm then the loops of the spiral will just touch; any larger and there will be areas between the loops which are not imaged. We modeled the diameter of the scanned area for different loop spacings; the results are shown in Fig. 6. The dotted line shows the settings chosen for the experimental results in the following section.

These results were computed by integrating over the length of the particular spiral defined by the required loop spacing and total time. The diameter was then taken as twice the radius of the final point of the spiral. A good approximation of these curves can be obtained if we note that the length L of a spiral of radius R and loop spacing Δr can be approximated by:

$$L \approx \frac{\pi R^2}{\Delta r}$$

If the spiral length is scanned in time t, with a frame rate F of 10 s^{-1} and a frame overlap of Δp, is given by $L = \Delta p \cdot F \cdot t$, then a first order approximation for the scan diameter D can be derived:

$$D \approx 2 \cdot \sqrt{\frac{\Delta r \cdot \Delta p \cdot F \cdot t}{\pi}}$$

The longest diameter of the resulting mosaic would be equal to $D - \Delta r/2$.

For the current configuration, the frame rate is 10 s^{-1} and we chose an image spacing Δp of 0.04 mm (as discussed above). If a continuous mosaic (i.e. a spiral without gaps between loops) was required, then the loop spacing Δr would need to be on the order of 0.2 mm, giving an approximate scan time $t \approx 10\ D^2$ seconds for a circle diameter of D mm. However, for the results presented below we set $\Delta r \approx 1$ mm, giving a more favourable $t \approx 2\ D^2$, albeit for a spiral that now contains gaps.

IV. Experimental Results

A. Mechanical performance

We first tested the mechanical performance of the 2-DOF scanning mechanism. The bending and rotation angles were evaluated against the target angles using a digital video camera. For the bending mechanism, measurements were performed in four parts: (a) bending from 0 degrees to +90 degrees, (b) returning to 0 degrees, (c) bending 0 to -90 degrees, and (d) returning again to 0 degrees (d). We repeated this set of measurements three times. Results are shown in Fig. 7(a). Similarly, for a test of the rotating mechanism the scanner was first rotated from 0 to 360 degrees (e), and then returned to 0 degrees (f), as shown in Fig. 7(b).

These results demonstrate that the prototype can successfully achieve ±90 degrees of bending and 360 degrees of rotation. Standard deviations of the measured angles were ±1.07 degrees for the bending motion and ±0.41 degrees for the rotational motion on average. The maximum hysteresis for bending was 4.54 degrees and for rotation was 1.79 degrees.

We then evaluated the trajectory of the tip using an NDI Aurora Electromagnetic Tracking System (NDI Corp, CA). A mini electromagnetic sensor with 6 DOFs was attached to the tip of the scanner, allowing its position to be measured. The trajectory of a full spiral scan is shown in Fig. 8. The trajectory shows that the scanner can cover a large area with a radius of 23 mm.

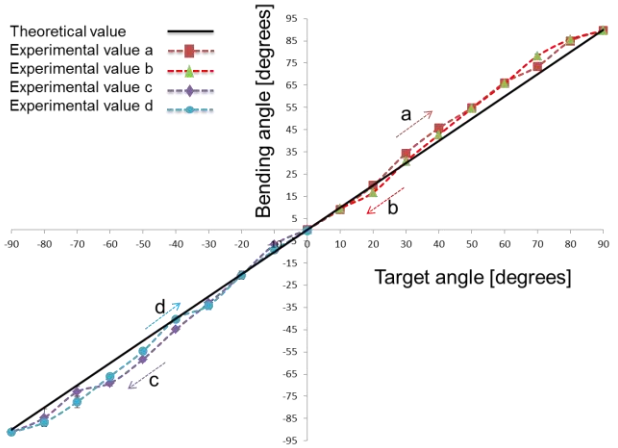

(a)

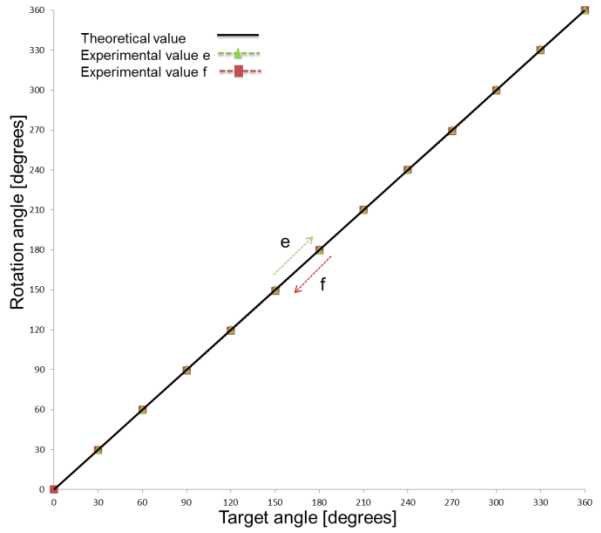

(b)

Figure 7. Results of 2DOF scanning characteristic test, showing relationship between target angles and actual bending and rotating angles. (a) 1-DOF bending mechanism, (b) 1-DOF rotating mechanism.

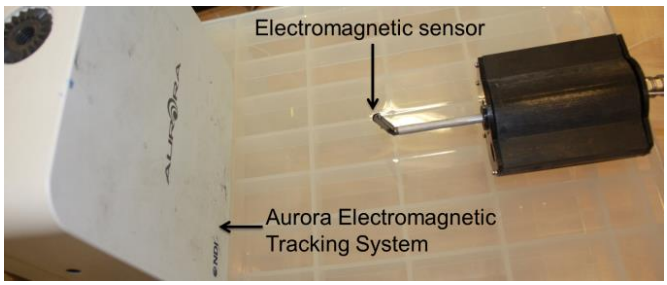

(a)

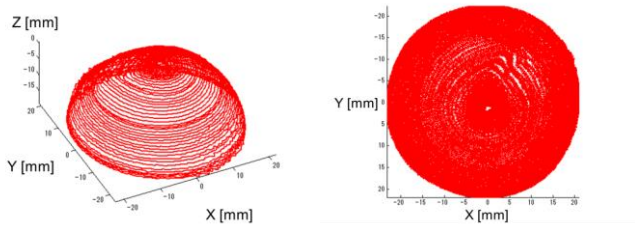

(b) (c)

Figure 8. Trajectory of a sample scan measured by the Aurora probe. (a) Setup for the experiment. (b) 3D trajectory of spiral scan, (c) 2D trajectory of spiral scan.

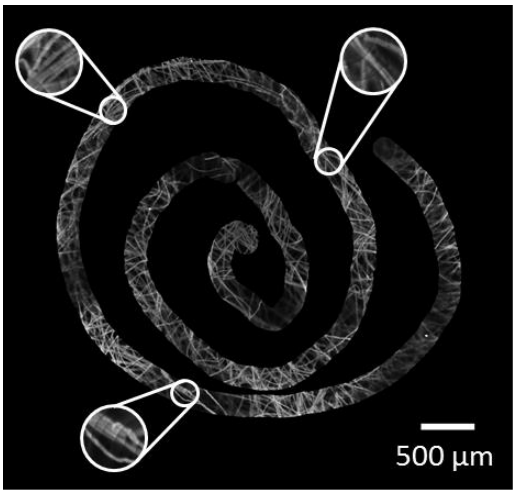

Figure 9. Mosaic created from large area spiral scan over lens tissue paper stained with acriflavine. Circled insets are shown at approximately 2.5X magnifcation. Stitching between individual frames is visible in the insets.

B. Image mosaicing

The prototype has the capability to scan over an area using various trajectories, such as linear scans, concentric circles and spiral scans. This was demonstrated by scanning a non-overlapping spiral pattern over a piece of lens tissue paper stained with acriflavine. The resulting mosaic is shown in Fig. 9. The scanner motors were controlled so as to maintain an approximately constant probe tip velocity of 0.4 mm/s, or a shift of approximately 40 µm between image frames. The spacing between loops of the spiral was set to approximately 1 mm, corresponding to the settings indicated by the dashed line in Fig. 6. This allowed the spiral to be scanned in 61 seconds, and a mosaic to be created from 610 image frames. Note that the diameter of the spiral is approximately 4 mm, somewhat smaller than would be predicted from Fig. 6, most likely due to a combination of mosaicing errors and deformation of the scanned surface. This diameter is also considerably smaller than the full scan range of the system for reasons we discuss below.

C. Ex vivo breast tissue experiments

We confirmed the ability of the system to obtain consistent *ex vivo* images from freshly excised, acriflavine-stained human breast cancer tissues. All subjects gave prior written informed consent and Human Tissue Authority licence and ethics approval were obtained from Imperial College Tissue Bank (R12047).

For this test we performed linear scans by driving only the bending motor and leaving the rotational position unchanged. This allowed us to obtain high quality mosaics using a simple, real-time normalized cross-correlation algorithm as we did not need to consider rotations. For this test we fixed the transparent membrane onto a support ring which was fixed to the rotational shaft of the scanner, as shown in Fig. 10(a). Fig. 10(b) shows mosaics of linear scans (approximately 5 mm in length) obtained over *ex vivo* human breast tissue.

V. Discussion

In this paper, we have proposed a large area scanner for breast endomicroscopy, and we confirmed that our prototype has a large workspace, high repeatability and small hysteresis. The distal end of the scanner enables bending between ±90 degrees, and rotation of 360 degrees, with repeatability of ±1.07 and ±0.41 degrees respectively. Backlash was reduced by a spring structure in the driver unit, which engages the rotation gear shaft against the spur gear link. The hysteresis between the rotation gear shaft and the spur gear link was small at a maximum of 4.54 degrees. This could be minimized further by increasing the precision of the gear on the rotation gear shaft.

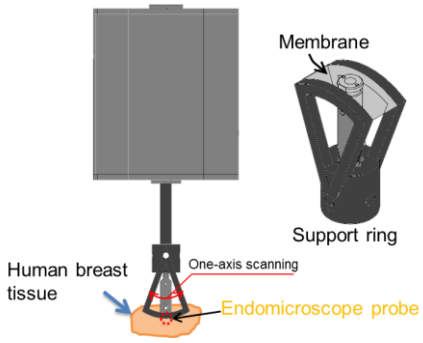

(a)

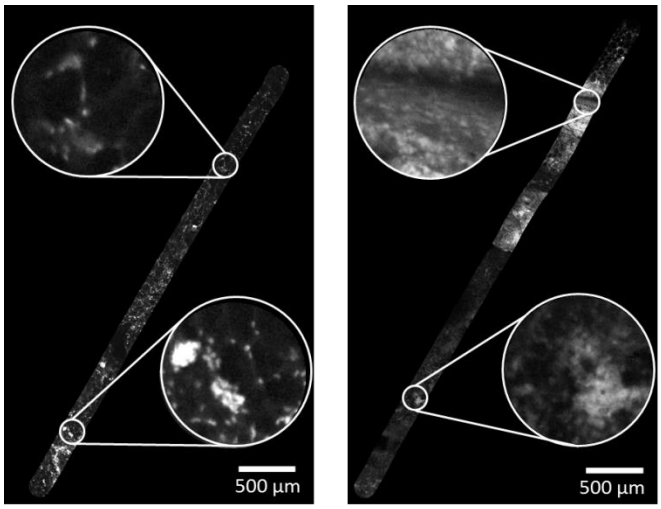

(b) (c)

Figure 10. Mosaic images, (a) Setup. (b) Human breast fat: numerous polygonal-shaped, dark-coloured cells with thin hyperfluorescent borders depicts the typical appearances of fat cells. (c) Human breast cancer: markedly disorganized architecture with hypercellularity and haphazard arrangement of cells. Circled insets are shown at approximately 6X magnification.

The trajectory experiment with the NDI Aurora Electromagnetic Tracking System showed that the distal end achieves a smooth large spiral scanning motion in 3D space when unloaded. The scan area was a hemispherical surface with a radius of 23 mm, which is considerably larger than for previously reported endomicroscopy scanners. However, forming a continuous mosaic over such a large area would be an interesting image processing problem which is being investigated separately. It may be preferable to instead create an array of smaller mosaic centered on user-specified points of interest. Such an approach can be easily accommodated by the proposed hardware design.

A further impediment to achieving a large area scan is the flexibility of the fibre bundle probes. We are not aware of minimum bending radius specified for the probe used here, but commonly used Fujikura fibre bundles have a minimum bending radius of the order of 70 mm (FIGH-30-800G). It is therefore unlikely that the full hemispherical scan could be achieved in practice. To resolve this issue, more flexible fibre bundles such as Schott leached imaging bundles, together with customized distal optics, need to be used.

To demonstrate the potential of the device to image over substantial areas of tissue we implemented a cross-correlation based mosaicing algorithm. Since the position and angle of each frame is determined by comparing it with the previous frame, this method accumulates errors during the scan. This would prevent a gap-free image from being generated, as it is unlikely that the loops of the spiral would correctly align. A more complex mosaicing algorithm would therefore be required for clinical use, one that uses positional feedback from the motor and takes account of tissue deformation. Given the likely high computational requirements of such an algorithm it may be necessary to implement a simpler, online version for provisional, real-time visualization, and a more complete, offline version for diagnostic purposes.

The *ex vivo* tissue evaluation in this study has shown that the scanner has strong potential to enable stable imaging from human breast tissue. A support ring with a membrane as an attachment was used to facilitate linear scanning. Together with the passive linear structure we found this to be a useful method for slightly reshaping the tissue surface to allow smooth scanning. The membrane could also be inflated by air or water and this could potentially conform irregular cavity surfaces to the smooth, spherical membrane surface, thereby aiding large area scanning of irregular surfaces.

VI. Conclusions

In this study, we have developed a scanning device to address the problems associated with scanning and mosaicing over large tissue areas in confocal endomicroscopy. This device was designed specifically for use during breast surgery, and so is substantially different from previously reported endomicroscopy scanners. By sacrificing the miniaturization required for flexible endoscopic use, our rigid device makes it possible to scan over a much larger spherical surface. This is achieved through use of a novel 2-DOF scanning mechanism, together with a passive linear structure for smoothing the tissue surface. We have demonstrated the creation of a mosaic over a substantial portion of the scanning workspace, demonstrating the potential to provide a much larger

field-of-view for 'optical biopsy' than has previously been possible. This could offer the surgeon much more comprehensive information than simple point imaging or short manual mosaics, greatly improving the prospects for intraoperative *in situ* cavity margin evaluation.

ACKNOWLEDGMENT

This work was supported by EPSRC grant EP/IO27769/1: SMART Endomicroscopy.

REFERENCES

[1] J. Ferlay, P. Autier, M. Boniol, M. Heanue, M. Colombet, and P. Boyle, "Estimates of the cancer incidence and mortality in Europe in 2006," Annals of oncology : official journal of the European Society for Medical Oncology / ESMO 18, pp. 581-592, 2007.

[2] G. F. Schwartz, U. Veronesi, K. B. Clough, J. M. Dixon, I. S. Fentiman, S. H. Heywang-Kobrunner, R. Holland, K. S. Hughes, R. E. Mansel, R. Margolese, E. B. Mendelson, I. A. Olivotto, J. P. Palazzo, and L. J. Solin, "Consensus conference on breast conservation," Journal of the American College of Surgeons 203, pp. 198-207, 2006.

[3] S. E. Singletary, "Surgical margins in patients with early-stage breast cancer treated with breast conservation therapy," American journal of surgery 184, pp. 383-393, 2002.

[4] B. Kreike, A. A. Hart, T. van de Velde, J. Borger, H. Peterse, E. Rutgers, H. Bartelink, and M. J. van de Vijver, "Continuing risk of ipsilateral breast relapse after breast-conserving therapy at long-term follow-up," International journal of radiation oncology, biology, physics 71, pp. 1014-1021, 2008.

[5] A. R. Miller, G. Brandao, T. J. Prihoda, C. Hill, A. B. Cruz, Jr., and I. T. Yeh, "Positive margins following surgical resection of breast carcinoma: analysis of pathologic correlates," Journal of surgical oncology 86, pp. 134-140, 2004.

[6] R. Jeevan, D. A. Cromwell, M. Trivella, G. Lawrence, O. Kearins, J. Pereira, C. Sheppard, C. M. Caddy, and J. H. van der Meulen, "Reoperation rates after breast conserving surgery for breast cancer among women in England: retrospective study of hospital episode statistics," BMJ 345, e4505, 2012.

[7] G. C. Balch, S. K. Mithani, J. F. Simpson, and M. C. Kelley, "Accuracy of intraoperative gross examination of surgical margin status in women undergoing partial mastectomy for breast malignancy," The American surgeon 71, pp. 22-27; discussion pp. 27-28, 2005.

[8] C. H. Lee and D. Carter, "Detecting residual tumor after excisional biopsy of impalpable breast carcinoma: efficacy of comparing preoperative mammograms with radiographs of the biopsy specimen," AJR. American journal of roentgenology 164, pp. 81-86, 1995.

[9] R. G. Pleijhuis, M. Graafland, J. de Vries, J. Bart, J. S. de Jong, and G. M. van Dam, "Obtaining adequate surgical margins in breast-conserving therapy for patients with early-stage breast cancer: current modalities and future directions," Annals of surgical oncology 16, pp. 2717-2730, 2009.

[10] J. C. Cendan, D. Coco, and E. M. Copeland, 3rd, "Accuracy of intraoperative frozen-section analysis of breast cancer lumpectomy-bed margins," Journal of the American College of Surgeons 201, pp. 194-198, 2005.

[11] J. M. Jabbour, M. a. Saldua, J. N. Bixler, and K. C. Maitland, "Confocal Endomicroscopy: Instrumentation and Medical Applications," Annals of biomedical engineering, 2011.

[12] S. Abeytunge, et al. "Confocal microscopy with strip mosaicing for rapid imaging over large areas of excised tissue." Journal of biomedical optics 18, 061227, 2013

[13] T. P. Chang, D. R. Leff, S. Shousha, D. J. Hadjiminas, R. Ramakrishnan, M. Gudi, R. Al-Mufti, M. R. Hughes, A. Darzi, and G. Z. Yang. "Imaging of breast cancer morphology using probe-based confocal laser endomicroscopy: Towards a novel imaging tool for real-time intra-operative cavity scanning," Eur J Surg Oncol. 2013 (abstract in press)

[14] M. Wallace, G. Y. Lauwers, Y. Chen, E. Dekker, P. Fockens, P. Sharma, and A. Meining, "Miami classification for probe-based confocal laser endomicroscopy," Endoscopy 43, pp.882-9, 2011.

[15] R. C. Newton, S. V. Kemp, G. Z. Yang, D. S. Elson, A. Darzi, and P. L. Shah, "Imaging parenchymal lung diseases with confocal endomicroscopy," Respiratory medicine 106, pp. 127-137, 2012.

[16] N. Ayache, T. Vercauteren, G. Malandain, F. Oberrietter, N. Savoire, and A. Perchant, "Processing and mosaicing of fibered confocal images," in Microscopic Image Analysis with Applications in Biology 2006.

[17] V. Becker, T. Vercauteren, C.H. von Weyhern, C. Prinz, R.M. Schmid, and A. Meining, "High-resolution miniprobe-based confocal microscopy in combination with video mosaicing (with video)," Gastrointest. Endosc., 66(5), pp.1001-1007, 2007.

[18] T. Vercauteren, "Image registration and mosaicing for dynamic in vivo fibred confocal microscopy," PhD Thesis, Ecole des Mines de Paris, Paris, France, 2008.

[19] N. Ayache, T. Vercauteren, G. Malandain, F. Oberrietter, N. Savoire, and A. Perchant, "Processing and mosaicing of fibered confocal images," in Microscopic Image Analysis with Applications in Biology 2006.

[20] D. P. Noonan, D. S. Elson, G. P. Mylonas, A. Darzi, and G. Z. Yang, "Laser-induced fluorescence and reflected white light imaging for robot-assisted MIS," IEEE transactions on biomedical engineering 56, pp. 889-92, 2009.

[21] B. Rosa, B. Herman, J. Szewczyk, B. Gayet, and G. Morel, "Laparoscopic optical biopsies: in vivo robotized mosaicing with probe-based confocal endomicroscopy," in Proc. of IROS'2011, San Francisco, California, September 25-30, 2011.

[22] M. S. Erden, B. Rosa, J. Szewczyk, and G. Morel, "Mechanical design of a distal scanner for confocal microlaparoscope: a conic solution," in Proc. of ICRA'2013, Karlsruhe, Germany, May 6-10, 2013.

[23] R. C. Newton, D. P. Noonan, V. Vitiello, J. Clark, C. J. Payne, J. Shang, M. Sodergren, A. Darzi, and G. Z. Yang. "Robot-assisted transvaginal peritoneoscopy using confocal endomicroscopy: a feasibility study in a porcine model," Surgical endoscopy 26.9, 2012.

[24] W. T. Latt, R. C. Newton, M. Visentini-Scarzanella, C. J. Payne, D. P. Noonan, J. Shang, and G. Z. Yang, "A hand-held instrument to maintain steady tissue contact during probe-based confocal laser endomicroscopy," IEEE transactions on biomedical engineering 58, pp. 2694-2703, 2011.

[25] P. Giataganas, V. Vitiello, V. Simaiaki, E. Lopez, and G. Z. Yang "Cooperative in situ microscopic scanning and simultaneous tissue surface reconstruction using a compliant robotic manipulator," in IEEE International Conference on Robotics and Automation (ICRA 2013).

[26] M. S. Erden, B. Rosa, J. Szewczyk, and G. Morel, "Understanding soft-tissue behavior for application to microlaparoscopic surface scan," IEEE transactions on biomedical engineering 60, pp. 1059-1068, 2013.

[27] T. Vercauteren, A. Perchant, G. Malandain, X. Pennec, and N. Ayache, "Robust mosaicing with correction of motion distortions and tissue deformations for in vivo fibered microscopy," Medical image analysis 10, pp. 673-692, 2006.

[28] B. Rosa, M. S. Erden, T. Vercauteren, B. Herman, J. Szewczyk and G.Morel. "Building large mosaics of confocal endomicroscopic images using visual servoing." IEEE transactions on biomedical engineering 60, pp. 1041-9, 2013.

[29] G. Goualher, A. Perchant, M. Genet, C. Cav, B. Viellerobe, B. Abrat, and N. Ayache, "Towards optical biopsies with an integrated fibered confocal fluorescence microscope," in Medical Imaging Computing and Computer Assisted Intervention (MICCAI), 2004.

[30] A. F. Gmitro and D. Aziz, "Confocal microscopy through a fiber-optic imaging bundle," Optics Letters 18, pp. 565-567, 1993.

[31] N. Bedard, T. Quang, K Schmeler, R. Richards-Kortum, T. Tkaczyk, "Real-time video mosaicing with a high-resolution microendoscope," Biomedical Optics Express 3, pp 2428-35, 2012.